Int. J. Electrochem. Sci., 8 **(2013)** 11564 - 11577

International Journal of
ELECTROCHEMICAL
SCIENCE
www.electrochemsci.org

Fabrication of Ni-CeO_2 Nanocomposite Coatings Synthesised via a Modified Sediment Co-Deposition Process

N.S Qu[1,2], *W.H. Qian*[1], *X.Y. Hu*[1], *Z.W. Zhu*[2]

[1] College of Mechanical and Electrical Engineering, Nanjing University of Aeronautics and Astronautics, Nanjing, China, 210016
[2] Jiangsu Key Laboratory of Precision and Micro-Manufacturing Technology, Nanjing, China, 210016
[*]E-mail: nsqu@nuaa.edu.cn

Received: 16 July 2013 / *Accepted:* 28 July 2013 / *Published:* 20 August 2013

It is well known that the amount and distribution of co-deposited nanoparticles play important roles in the properties of the nanocomposite coatings. Therefore improvement of the incorporated nanoparticle content in nanocomposite coatings is a crucial factor in the composite electrodeposition process. In this study, a modified sediment co-deposition (SCD) technique was developed to produce Ni-CeO_2 nanocomposite coatings with a high content of incorporated CeO_2 nanoparticles. In this technique, the electrolyte flows through the gap between the cathode and the anode. Compared with the standard SCD, the modified process is of benefit to large-area electrodeposited coatings because the electrolyte flows through the cathode surface at the same rate, and the bubbles absorbed onto the cathode surface can escape from the cathode surface due to shock from the composite electrolyte during the modified SCD process. The effects of current density and the CeO_2 nanoparticle content in the bath on the morphology, preferred orientation, microhardness, and wear resistance of nanocomposite coatings obtained from the modified SCD are investigated. The experimental results show that the weight per cent of CeO_2 particles in the nanocomposite coatings varies with increasing loading of CeO_2 nanoparticles and current density. The maximum weight per cent of CeO_2 particles in the nanocomposite coatings (6.30 wt%) is obtained at a current density of 1 A dm^{-2} using a concentration of 30 gl^{-1} of CeO_2 particles in the bath, and this maximum is significantly higher than that of coatings fabricated using the conventional electrodeposition technique. The surface morphology and preferred orientation are altered with the incorporation of CeO_2 nanoparticles. A Ni-CeO_2 nanocomposite coating with a maximum microhardness of 630 HV is obtained from this process. The Ni–CeO_2 nanocomposite coatings show increased wear resistance compared with that of the pure Ni coating, whereas the composite coating with the highest CeO_2 content exhibits the best wear resistance.

Keywords: composite electrodeposition, sediment co-deposition, CeO_2 nanoparticles, microhardness, wear resistance

1. INTRODUCTION

Metal matrix nanocomposite coatings consist of a metallic matrix strengthened by the addition of nano-sized metallic or nonmetallic particles (or whiskers). These materials often exhibit enhanced physical, mechanical, and chemical properties compared with those of the bulk material coatings [1-3]. Nanocomposite coatings offer novel properties, such as increased toughness, high temperature inertness, chemical and biological compatibility, magnetism, piezoelectricity and photochromatism [4-6]. The synthesis and characterisation of metal-matrix nanocomposite coatings have attracted increasing attention in recent years. Electrodeposition is one method used to prepare metal-matrix nanocomposite coatings. In this process, the nanoparticles (or whiskers) are suspended in an electrolyte and embedded in the growing metal layer [7]. Nano-sized particles dispersed into a metal matrix can promote homogeneity of the composites and expand the potential applications for metal matrix nanocomposite coatings. Different types of nanostructure composites (i.e., Ni-SiC, Ni-Al_2O_3, Ni-ZrO_2, Cu-Al_2O_3, Ni-P-Carbon nanotubes, Ni-diamond, etc.) have been successfully prepared to improve the wear resistance, corrosion resistance, and high-temperature oxidisation resistance, and other properties. [8-13]. Nano-sized inert particles that are well dispersed in a metal matrix not only enhance the mechanical properties but also open up potential applications of the composite materials for microdevices. For example, Hung developed a NiCo-Al_2O_3 nanocomposite micro-mold for a micro-lens array prepared using LIGA [14].

Nickel is one of the most commonly used structural metals for various engineering applications, and nickel coating can be used to provide resistance to corrosion, erosion and abrasion. To improve these properties, reinforced nickel composite coatings have been developed for particles. The Ni-SiC composite coatings exhibit good corrosion resistance and wear resistance properties and have been successfully applied in the automobile industry [15]. Rare earth oxides have been widely used in electronics and materials and chemical engineering due to their special characteristics [16, 17]. As one of the rare earth oxides, cerium oxide (CeO_2) has attracted considerable interest as a promising material in anti-wear coatings, solid fuel electrolyte applications, environmental catalysis, abrasive chemical mechanical polishing, and other applications. Electrodeposition is an attractive method for the preparation of thin films of CeO_2-reinforced metal-matrix composites. Campos et al. synthesised Pt-CeO_2 composite coatings via electrodeposition [18], Carac et al. produced Ni-Co-CeO_2 composite coatings by electrodeposition [19], Mitoseriu et al. prepared Cu-CeO_2 composite coatings by electrodeposition [20], and Balathandan et al. reported that an Ni matrix reinforced with micron-sized CeO_2 particles displayed good corrosion resistance compared with that of Ni-ZrO_2, Ni-PSZ, and pure Ni coatings [21]. Yu et al. produced Ni-P-CeO_2 nanocomposite coatings by electroless plating that exhibited excellent corrosion resistance [22]. Meenu et al. found that NiCo–CeO_2 nanocomposite coatings enhanced the microhardness, wear resistance and thermal stability [23], and Aruna et al. demonstrated that the microhardness of the Ni matrix was enhanced by incorporation of CeO_2 nanoparticles [24]. It was also demonstrated that the friction and wear behaviours of Ni–CeO_2 composite coatings are closely related to the CeO_2 particle content [25].

It is well known that the amount and distribution of co-deposited nanoparticles play important roles in the properties of the nanocomposite coatings. Sufficient incorporation percentages and more

uniform distribution of nanoparticles in the nanocomposite coatings lead to improvement of the mechanical, tribological, anti-corrosion, and anti-oxidation properties of the coatings [26]. Thus, much attention has been focused on improvement of the incorporated nanoparticle content in the nanocomposite coatings. Studies show that application of a surfactant might favour a greater amount of uniformly distributed nanoparticles in the electrodeposited coatings [27, 28]. Baghal et al. indicated that the addition of SDS to Ni–Co electrolyte increased the amount and improved the uniform distribution of SiC nanoparticles in the deposits [28]. The sediment co-deposition (SCD) technique (shown in Figure 1) has been proven as an effective method for increasing the particle incorporation. In this technique, periodic stirring is applied to allow improved particle suspension in the electrolyte and sediment deposition on the cathode, and the force of gravity provides an additional tendency for particle settling [29,30]. Bakhit and Akbari prepared Ni–Co/SiC nanocomposite coatings with 8.1 vol.% SiC nanoparticles incorporated via the SCD technique [29], and Feng et al. reported that the wear resistance for SCD-produced composite coatings is superior to that obtained from conventional electroplating techniques [30].

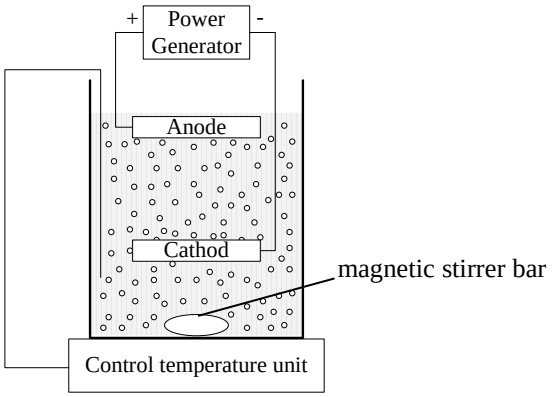

Figure 1. Schematic diagram of the sediment co-deposition technique

In this study, the modified SCD technique shown in Figure 2 was developed to produce Ni-CeO_2 nanocomposite coatings with a high content of incorporated CeO_2 nanoparticles. In this technique, the electrolyte flows through the gap between the cathode and the anode. Compared with the standard SCD technique, the modified process is of benefit to large-area coatings because the electrolyte flows through the cathode surface at the same rate as during the modified SCD process, whereas the electrolyte flows through the cathode surface at a different rate during the standard SCD. Furthermore, the bubbles absorbed onto the cathode surface can escape from the cathode surface due to the shock from the composite electrolyte during the modified SCD process, which is of benefit to the coating surface roughness. This work described in this study investigates the effect of current density and the CeO_2 nanoparticle content in the bath on the morphology, preferred orientation, microhardness, and wear resistance of Ni-CeO_2 nanocomposite coatings obtained from the modified SCD process.

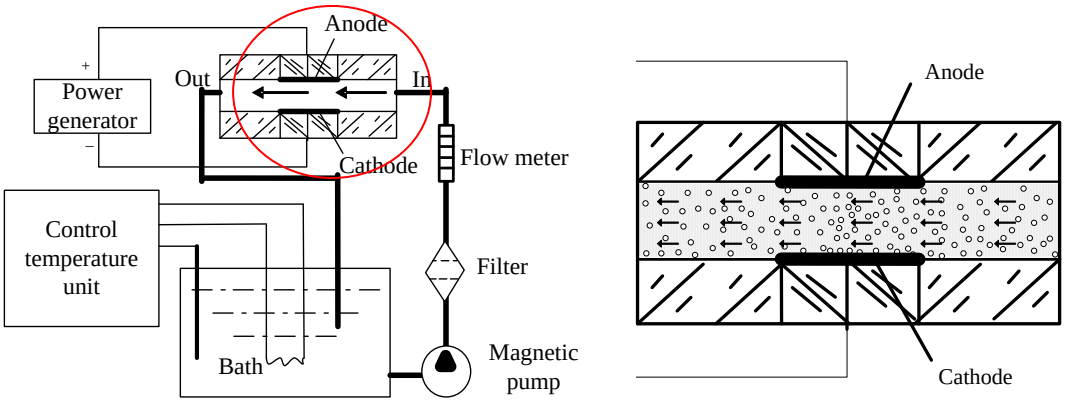

Figure 2. Schematic diagram of the modified co-deposition process

2. EXPERIMENTAL

Figure 2 shows the schematic diagram of the experimental set-up, which consists of a magnetic pump, an electrolyte bath, a power generator, an electrolytic cell, and a temperature control unit. In the electrolytic cell, the cathode and anode are positioned in parallel with a gap distance of 2 mm, and the electrolyte flows through the gap. An insoluble platinum plate with dimensions of 70 mm × 60 mm × 3 mm was applied as the anode, and a stainless steel specimen with dimensions of 70 mm × 60 mm × 1 mm was employed as the cathode and grounded with grade-400 emery papers. In the experiments, the bath consisted of 350 gl^{-1} nickel sulphamate, 15 gl^{-1} ammonium chloride, 35 gl^{-1} boric acid, and 0.1 gl^{-1} sodium dodecyl sulphate. The bath temperature was maintained at 50±1ºC. Particle of CeO_2 with a mean diameter of 20-30 nm were added into the electrolyte. To ensure that the nano-sized particles were uniformly dispersed, the electrolyte was pumped from the tank into the inter-electrode gap for 120 min prior to the deposition process.

The deposition thickness for each experiment was fixed at 50 μm by altering the deposition time. The surface morphology of the deposited nickel was examined via scanning electron microscope (S3400N Hitachi, Japan), and the preferred orientation of the deposits was examined by X-ray diffraction (D8 Advance 40 kV, 40 mA, Bruker, Germany). The percentage of embedded particles in the deposits was determined by the energy dispersive spectrum (X-Flash5010, Bruker, Germany). The microhardness of the nanocomposite coatings was measured via a microhardness tester (HXS—1000A, Shanghai Shangguang Instrument Plant, China) with a loading force of 100 g. Five measurements were taken from each sample, and an average microhardness value was calculated. In the wear resistance test, the counter-body was constructed from 404L stainless steel with a hardness of HRC 63. The experimental parameters were selected as follows: applied load = 4.98 N, frequency = 2.5 Hz, and time = 10 min. All experiments were conducted at room temperature without any lubrication.

3. RESULTS AND DISCUSSION

3.1 Morphology and composition of coatings

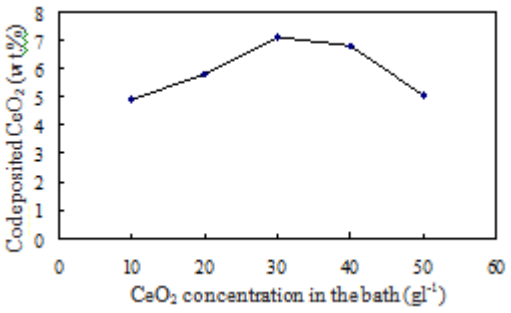

Figure 3. Effect of CeO_2 nanoparticle content in the electrolyte on the weight per cent of CeO_2 particles incorporated in the coatings

Figure 3 shows the influence of the CeO_2 nanoparticle concentration in the bath on the content of CeO_2 embedded in the nanocomposite coatings at a current density of 1 A dm^{-2}. The incorporated CeO_2 particle content was measured via the CeO_2 weight fraction calculated from the content of the corresponding Ce measured from the energy dispersive spectroscopy results of the corresponding samples. The weight per cent of CeO_2 particles incorporated in the deposit increases when the CeO_2 particle concentration in the bath increases from 10 gl^{-1} to 30 gl^{-1} and subsequently decreases when the CeO_2 particle concentration in the bath further increases from 30 gl^{-1} to 50 gl^{-1}. The weight per cent of CeO_2 particles incorporated in the deposit is 4.90 wt% with an addition to the bath of 10 gl^{-1} of CeO_2 nanoparticles, and the maximum particle incorporation of 7.09 wt% CeO_2 is observed in nanocomposite coatings deposited with the addition of a nanoparticle concentration of 30 gl^{-1} CeO_2 to the bath. The CeO_2 particle content incorporated into the nanocomposite coatings was reduced to 5.04 wt% when the CeO_2 particle concentration was further increased to 50 gl^{-1}. A similar phenomenon was reported by Shi et al. for the fabrication of Ni–SiC nanocomposite coatings [31].

Guglielmi reported two mechanisms of composite electrodeposition [32]. In the first step, particles are transported to the cathode surface and are adsorbed weakly at the cathode via van der Waals forces, and in the second step, the particles are adsorbed strongly on the cathode via Coulombic forces and buried in the surrounding metal deposits. The nanoparticles adsorbed weakly at the cathode surface can be desorbed if they are struck by other particles transported by the pump in a bath with high particle concentration; as a result, the incorporated particle content in the composite coating would therefore decrease. An optimum nanoparticle concentration exists that allows the maximum weight per cent of CeO_2 nanoparticles to embed into the composite coatings. During variation from 5 gl^{-1} to 30 gl^{-1}, it was reported that the optimum particle bath concentration that yields the maximum co-deposition in the formation of Ni–SiC nanocomposite coatings is 20 gl^{-1} [31].

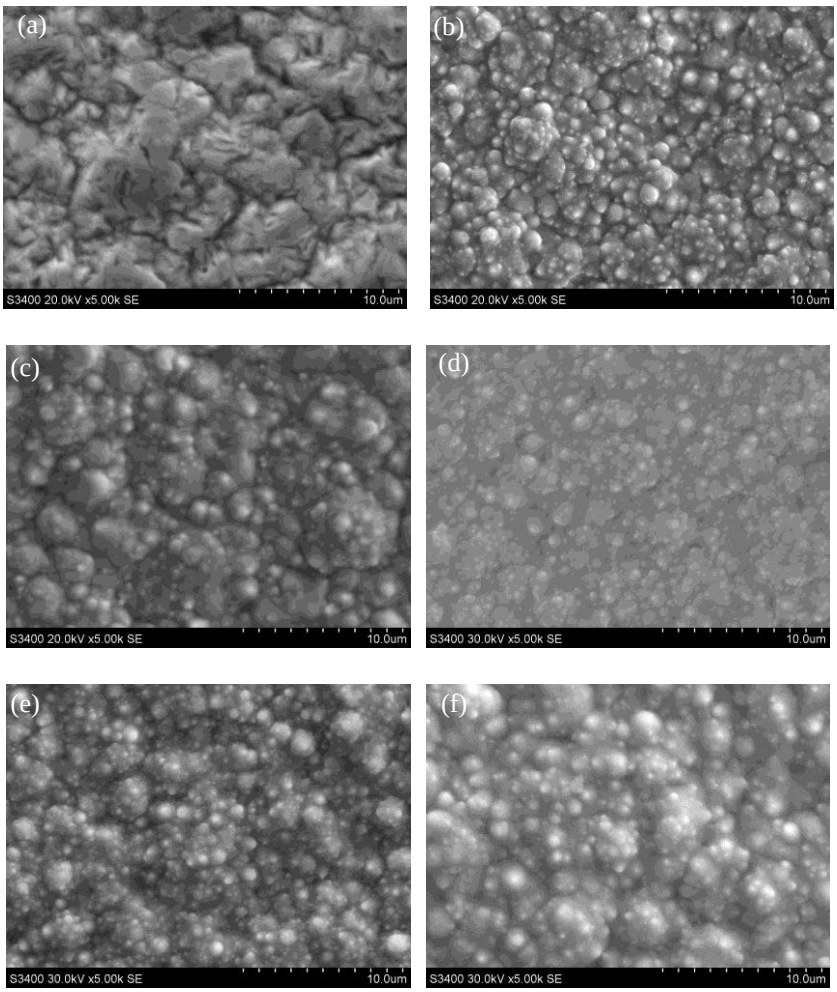

Figure 4. Morphology of Ni–CeO_2 nanocomposite coatings at a current density of 1 A dm^{-2} with various CeO_2 particle concentrations in the bath: (a) 0 gl^{-1}, (b) 10 gl^{-1}, (c) 20 gl^{-1}, (d) 30 gl^{-1}, (e) 40 gl^{-1}, (f) 50 gl^{-1}

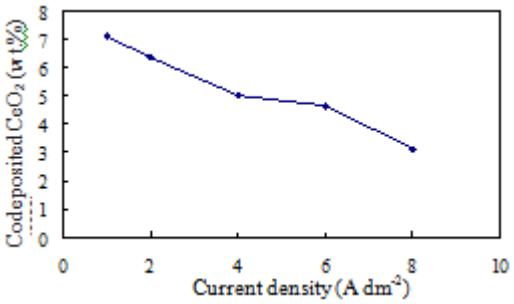

Figure 5. Effect of current density on the weight per cent of CeO_2 particles in the coatings

Figure 4 illustrates the surface morphologies of pure nickel coatings and Ni–CeO_2 nanocomposite coatings synthesised at a current density of 1 A dm^{-2} with different CeO_2 particle concentrations in the bath and shows that the surface morphologies were influenced by the CeO_2 particles in the bath. As shown in Figure 4(a), a pyramid structure is observed at the surface of the pure nickel. With the addition of CeO_2 particles, the grain size is reduced and the morphology changes to a

hemispherical grain structure, as shown in Figure 4(b)-(f). It appears that the coating surfaces become smoother when the CeO_2 particle concentration in the bath increases from 10 gl^{-1} to 30 gl^{-1}. However, a rough composite surface is observed when the CeO_2 particle concentration in the bath increases from 30 gl^{-1} to 50 gl^{-1}. It is worth noting that the smoothest surface coating is obtained when the weight per cent of CeO_2 nanoparticles embedded in the nanocomposite coatings is the largest.

The influence of the current density on the weight per cent of CeO_2 particles in the coatings is shown in Figure 5. This figure reveals that the weight per cent of CeO_2 particles in the coatings decreases with increasing current density. As the current density increases, a high deposition rate is obtained for nickel cations because the rate of movement of the nickel ions from the bulk solution to the cathode surface increases. However, the rate of incorporation of suspended CeO_2 particles is unchanged with increasing current density. As a result, it was concluded that the optimum current density in this investigation was 1 A dm^{-2}.

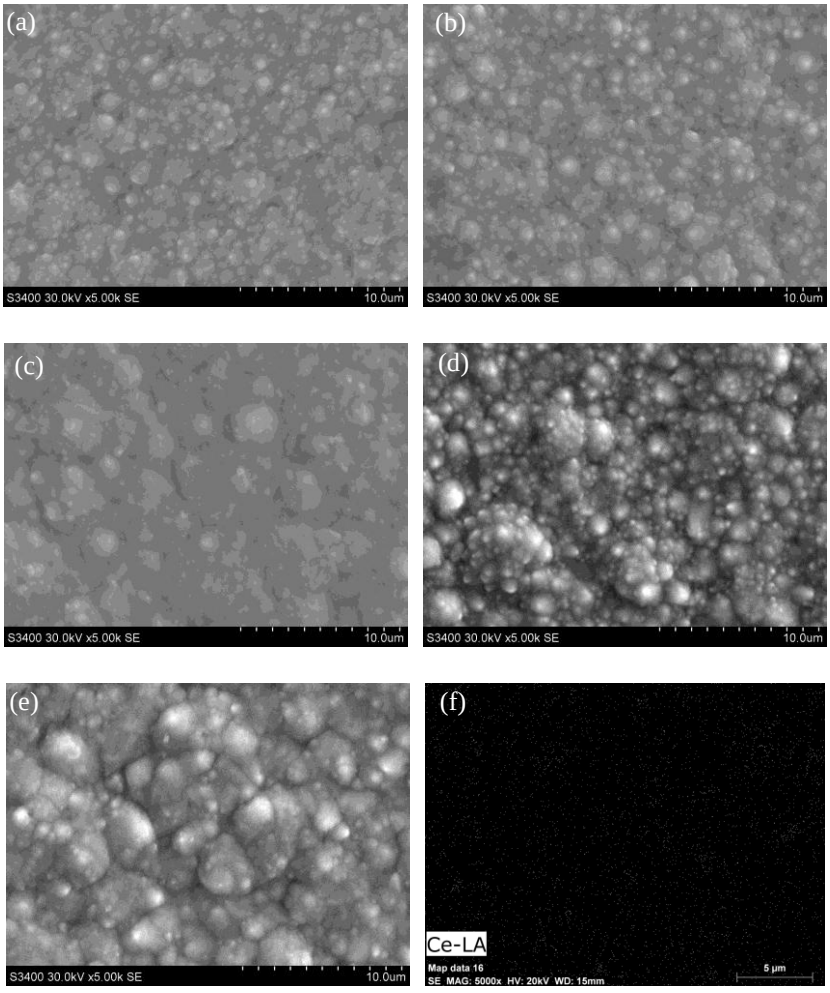

Figure 6. The morphology of Ni–CeO_2 nanocomposite coatings with a loading of 30 gl^{-1} CeO_2 nanoparticles at different current densities: (a) 1 A dm^{-2}, (b) 2 A dm^{-2}, (c) 4 A dm^{-2}, (d) 6 A dm^{-2}, (e) 8 A dm^{-2}, (f) Ce mapping of (a).

Figure 6 presents the morphologies of the Ni–CeO_2 nanocomposite coatings prepared at different current densities with a concentration of 30 gl^{-1} CeO_2 particles in the bath. This figure shows

that a rough surface is obtained on the composite coatings with increasing current density. Figure 6(f) shows the mapping of the Ce element in Figure 6(a) and indicates that a uniform distribution of the CeO_2 nanoparticles can be obtained in the Ni–CeO_2 nanocomposite.

In the electrodeposition process, the incorporation of CeO_2 particles into the coating can result in: (a) an increase in the electrocrystalline potential because the incorporated nanoparticles decrease the electrical cathode surface and (b) the occurrence of new nuclei because the adsorbed nanoparticles limit the growth of the original crystal grains. Both of these factors are considered favourable for fine grains and good surface morphology of the composite coatings.

3.2 Preferred orientation of coatings

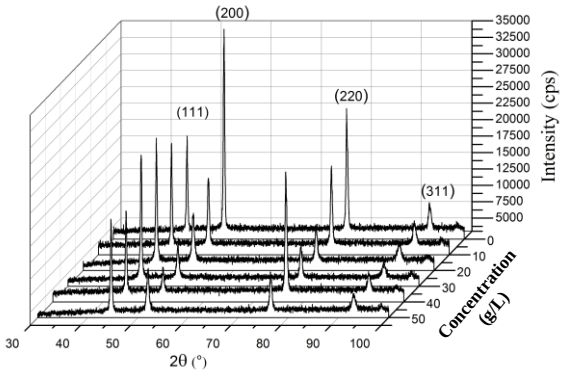

Figure 7. Effect of CeO_2 particle concentration in the electrolyte on the XRD patterns of the composite coatings

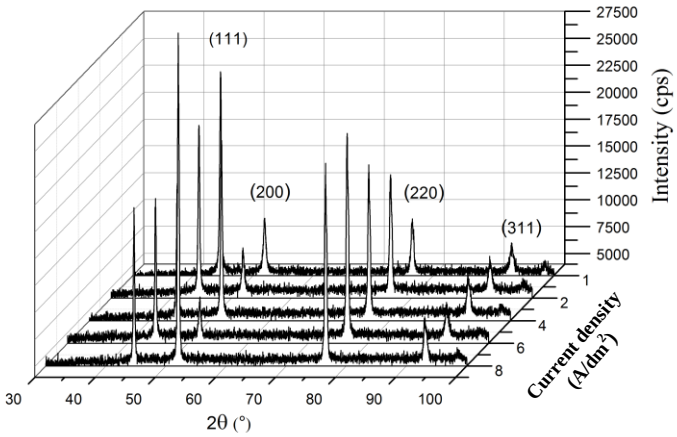

Figure 8. Effect of current density on the XRD patterns of the composite coatings

Figure 7 compares the XRD data for both pure nickel and Ni–CeO_2 nanocomposite coatings produced at a current density of 1 A dm^{-2} with varying CeO_2 particle content in the bath. For pure nickel, the relative intensity of the (200) orientation is much greater than that of other orientations, i.e., (111), (220), and (311), whereas with the addition of CeO_2 nanoparticles, a significant increase is

observed in the relative intensity of the (111) and (220) orientations. The XRD patterns of Ni–CeO_2 nanocomposite coatings prepared at various current densities with a 30 gl^{-1} CeO_2 particle concentration in the bath are shown in Figure 8. At a current density of 1 A dm^{-2}, the relative intensities of the (111), (200), and (220) peaks predominate. With an increase in the current density, the relative intensities of the (111) and (220) peaks predominate.

The electrocrystallisation of nickel is known to be a highly inhibited process, and the (100) preferred orientation is believed to result from a bath free of inhibiting chemical species. However, it is impossible for crystal growth to be completely free from inhibiting species, and certain species (i.e., hydrogen and nickel hydroxide) that exist in nickel electroplating play a major role in crystal growth. The change of preferred orientation is therefore attributed to a change in the inhibiting species under different conditions [34]. Additionally, boric acid is ionised according to the following reaction:

$$B(OH)_3+H_2O \Leftrightarrow [B(OH)_4]^-+H^+ \quad (1)$$

The CeO_2 particles in the bath can adsorb the Ni^{2+} and $Ni[B(OH)_4]^+$ cations, and the adsorbed cations are attracted to the growth centres that carry the CeO_2 particles, which will shield the growth centre from the cations of the electrolyte and preclude further growth of the grain. In this instance, re-nucleation must occur, and the preferential location for this process occurs on both the (111) and (220) faces [35]. However, the inhibitor species is not sufficient to affect the electrocrystallisation of all grains, and the (200) preferred orientation also exists. Therefore, all three types of preferred orientations, i.e., (111), (200), and (220), can occur in the nanocomposite coating.

3.3 Microhardness of coatings

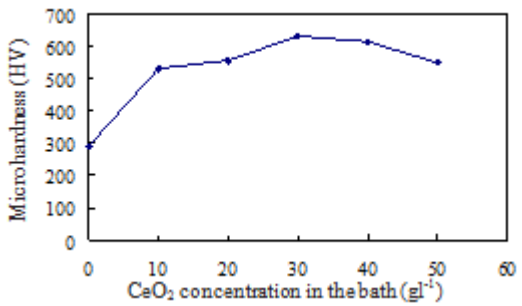

Figure 9. Effect of the CeO_2 particle concentration in the electrolyte on the microhardness of Ni – CeO_2 composite coatings

Figure 9 displays the microhardness of both pure nickel and Ni–CeO_2 nanocomposite coatings produced at a current density of 1 A dm^{-2} with different CeO_2 particle concentrations in the bath. The microhardness of pure nickel is approximately 291 HV. With an addition of 10 gl^{-1} of CeO_2 nanoparticles, the microhardness of the deposit increases significantly to 530 HV. The microhardness of the coatings is shown to increase when the CeO_2 particle concentration in the bath increases from 10 gl^{-1} to 30 gl^{-1} and subsequently decreases when the CeO_2 particle concentration in the bath increases from 30 gl^{-1} to 50 gl^{-1}. The maximum microhardness of 630 HV is observed in nanocomposite coatings

deposited with a CeO_2 nanoparticle bath concentration of 30 gl^{-1}. The variations in the microhardness and the weight per cent of CeO_2 nanoparticles embedded in composite coatings are similar, which is consistent with the findings reported by Malfatti et al. in the fabrication of NiP–SiC nanocomposite coatings [36]. The effect of current density on the microhardness of the composite coatings is shown in Figure 10, which shows that the microhardness of composite coatings decreases with increasing current density. In the current study, although the microhardness of pure nickel is nearly the same as that of previous reports, the maximum microhardness of the composite coatings is obviously higher than that fabricated using the conventional electrodeposition technique due to the high CeO_2 nanoparticle content incorporated in the composite coatings [33].

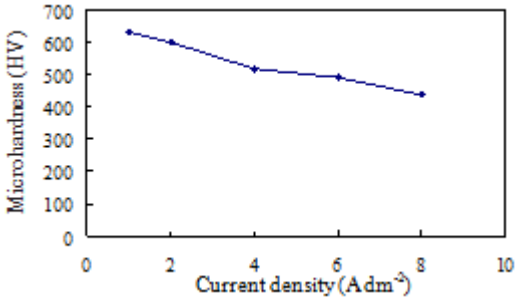

Figure 10. Effect of current density on the microhardness of Ni –CeO_2 composite coatings

The improved microhardness of the Ni–CeO_2 composite coatings is due not only to the strengthening effects of the CeO_2 particles but also to the modified nickel microstructure. It is known that the microstructure of the electrodeposit is refined when nanoparticles are embedded, and this refinement will increase the load-carrying capacity and improve the resistance to plastic deformation. Nanoparticles will also hinder the movement of dislocations, which will increase the microhardness of the composite and suppress the re-crystallisation and growth of crystal grains. Because the electrodeposition parameters affect the amount of CeO_2 nanoparticles incorporated in the nanocomposite, it may be possible to produce composite coatings with different microhardness values via control of the electrodeposition parameters.

3.4 Wear resistance of coatings

Figure 11 shows both the friction coefficient and wear weight loss of composite coatings synthesised at a current density of 1 A dm^{-2} with varying concentrations of CeO_2 particles in the electrolyte. Figure 11(a) indicates that the friction coefficient of the Ni–CeO_2 composite coatings is smaller than that of electrodeposited pure Ni. The lowest friction coefficient of 0.07 is observed in Ni–CeO_2 nanocomposite coatings obtained with the addition of 30 gl^{-1} of CeO_2 particles to the bath. The pure Ni coating displays the maximum wear weight loss, whereas the wear weight loss of the Ni–CeO_2 composite coating is reduced with the addition of CeO_2 particles to the bath, as observed in Figure 11(b). The wear weight loss of the Ni–CeO_2 composite coatings is reduced when the CeO_2 particle

content in the bath increases from 10 gl^{-1} to 30 gl^{-1} and subsequently increases when the CeO_2 particle content in the bath increases from 30 gl^{-1} to 50 gl^{-1}. The lowest wear weight loss for the Ni–CeO_2 composite coatings was found to occur with a CeO_2 particle content of 30 gl^{-1}.

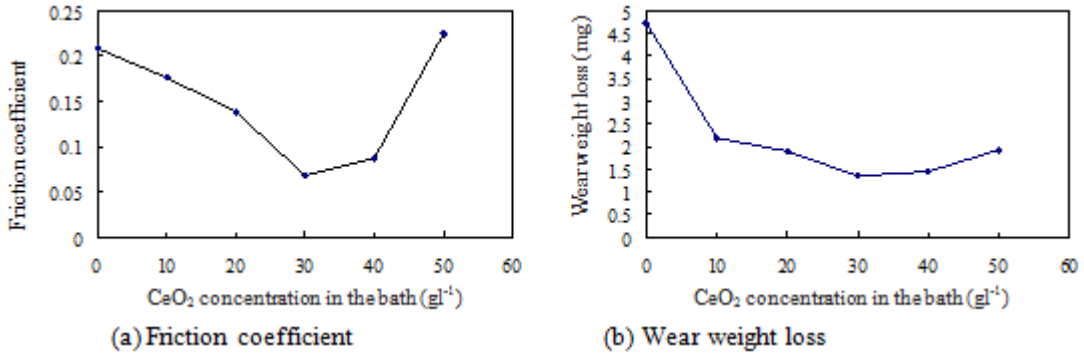

Figure 11. Effect of the CeO_2 particle concentration in the electrolyte on the friction coefficient and wear resistance of Ni-CeO_2 nanocomposite coatings prepared at a current density of 1 A dm^{-2}

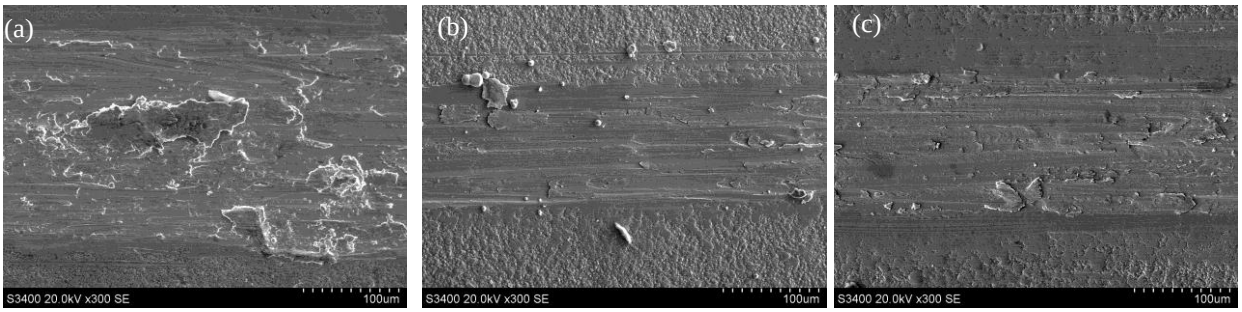

Figure 12. SEM image of the worn surfaces of pure Ni and Ni–CeO_2 composite coatings obtained at a current density of 1 A dm^{-2} with varying CeO_2 particle concentration in the bath: (a) 0 gl^{-1}, (b) 30 gl^{-1}, (c) 50 gl^{-1}

Figure 12 displays the morphology of the worn surface of the pure Ni and the Ni–CeO_2 composite coatings prepared at a current density of 1 A dm^{-2} with varying concentrations of CeO_2 particles in the bath. For the pure Ni coating, cracking and spalling can be observed on the worn surface, as shown in Figure 12(a), and the presence of cracking and spalling yields larger wear debris. This observation reveals that in the absence of CeO_2 particles in the Ni deposit, the wear resistance of the pure Ni coating is rather weak. Figure 12(b) shows that a trace of spalling with smaller width and depth on the worn surface of the Ni–CeO_2 composite coating obtained with the addition of 30 gl^{-1} CeO_2 particles in the bath. Furthermore, increasing the concentration of CeO_2 particles in the bath to 50 gl^{-1} causes the width of the spalling trace to increase on the worn surface of the Ni–CeO_2 composite coating, as shown in Figure 12(c).

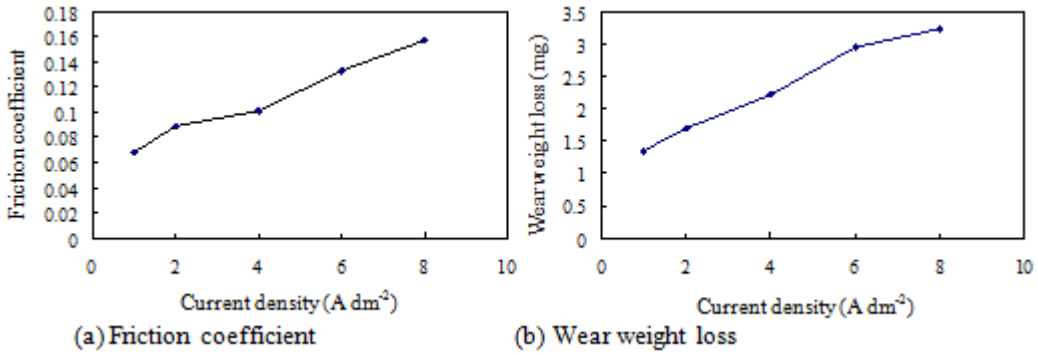

Figure 13. Effect of current density on the friction coefficient and wear resistance of Ni-CeO_2 nanocomposite coatings obtained with 30 gl^{-1} CeO_2 particles in the bath

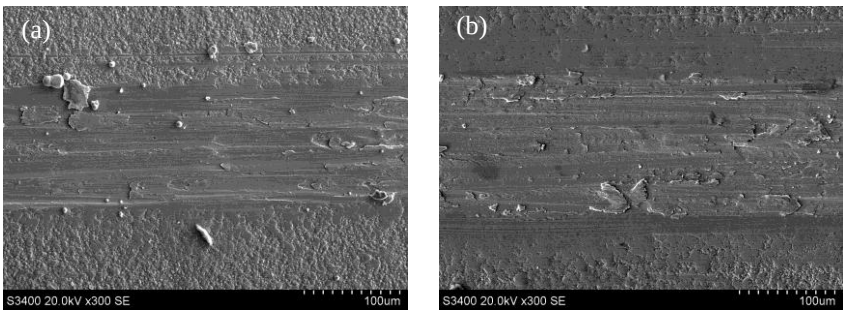

Figure 14. SEM image of the worn surfaces of the Ni –CeO_2 composite coatings obtained at a current densities of 1 A dm^{-2} and 8 A dm^{-2} with 30 gl^{-1} CeO_2 particles in the bath

Figure 13 shows both the friction coefficient and wear weight loss values for composite coatings synthesised at different current densities in a bath containing 30 gl^{-1} of CeO_2 particles. The figure shows that the friction coefficient of the Ni–CeO_2 composite coatings increases gradually with increasing current density, and the wear weight loss of the Ni–CeO_2 composite coatings increases with increasing current density. The morphology of the worn surface of the Ni–CeO_2 composite coatings prepared at current densities of 1 A dm^{-2} and 8 A dm^{-2} is shown in Figure 14. Compared with the worn surface of the Ni–CeO_2 composite coating obtained at a current density of 1 A dm^{-2}, a larger width was observed on the worn surface of the Ni–CeO_2 composite coating obtained at a current density of 8 A dm^{-2}.

The changes in the wear resistance of nanocomposite coatings obtained with different electrodeposition parameters could be attributed primarily to the incorporation of CeO_2 nanoparticles into the film because the CeO_2 nanoparticles provide both dispersion-strengthening and particle-strengthening, according to similar works in the literature [37]. During the friction process, the co-deposited CeO_2 nanoparticles gradually protrude out of the matrix and carry the loads transferred from the matrix. As a result, the wear resistance of Ni–CeO_2 composite coatings is enhanced. The increased content of well-distributed CeO_2 nanoparticles in the Ni matrix indeed mutually supports the enhancement of wear resistance. Additionally, the CeO_2 nanoparticles may act as a solid lubricant

between the contact surfaces, decreasing the friction coefficient and abating the wear on the composite coatings. An additional advantage is that such a solid lubricant (CeO_2) might further reduce the wear loss of the counterpart material. The loading–bearing capacity and the wear-reducing effects of the CeO_2 particles are closely related to the CeO_2 particle content in the composite coatings. Thus, the wear resistance of the Ni–CeO_2 composite coatings is enhanced with increasing CeO_2 particle content in the deposit.

4. CONCLUSIONS

In this work, a modified SCD technique was developed, and Ni-CeO_2 nanocomposite coatings with high CeO_2 particle contents were successfully produced using this technique. According to the experimental results, the following conclusions can be drawn.

(1) The weight per cent of CeO_2 particles in the nanocomposite coatings increases with an increases in the loading of CeO_2 nanoparticles from 10 gl^{-1} to 30 gl^{-1}. With further increase in the CeO_2 nanoparticle concentration to 40 gl^{-1}, the weight per cent of CeO_2 particles in the nanocomposite coatings is reduced. This value also decreases when the current density increases from 1 A dm^{-2} to 8 A dm^{-2} at a concentration of 30 gl^{-1} CeO_2 nanoparticles in the bath. The maximum weight per cent of CeO_2 particles in the nanocomposite coatings (6.30 wt%) is obtained at a current density of 1 A dm^{-2} with the addition of 30 gl^{-1} CeO_2 particles, a value that is obviously higher than that fabricated using the conventional electrodeposition technique.

(2) With the incorporation of CeO_2 nanoparticles, the morphology and preferred orientation of the composite coatings are altered.

(3) The data indicate that the microhardness is enhanced with an increase in the CeO_2 nanoparticles incorporated into the metal matrix. A Ni-CeO_2 nanocomposite coating with a maximum microhardness of 630 HV is obtained, a value that is obviously higher than that fabricated using the conventional electrodeposition technique.

(4) The friction and wear behaviours of Ni–CeO_2 nanocomposite coatings are closely related to both the current density and CeO_2 nanoparticle concentration in the bath. The Ni–CeO_2 nanocomposite coatings show a somewhat increased wear resistance compared with that of the pure Ni coating, and the composite coating with the highest CeO_2 content shows the best wear resistance.

ACKNOWLEDGEMENT
The work described in this study was supported by the Joint Funds of the National Natural Science Foundation of China and Guangdong Province (grant no. U1134003).

References

1. E. M. Moustafa, A. Dietz, T. Hochsattel, *Surf. Coat. Technol*. 216 (2012) 93
2. D. Thiemig, A. Bund, J. B. Talbot, *Electrochim. Acta*. 54 (2009) 2491
3. W. Shao, D. Nabb, N. Renevier, I. Sherrington, J. K. Luo, *J. Electrochem. Soc*. 159 (2012) D671

4. S. Pane´a, E. Go´mez and E. Valle´s, *Electrochem. Commun*. 9 (2007) 1755
5. S. K. Mishra, P. Mahato, B. Mahato, L. C.Pathak, *Appl. Surf. Sci*. 266 (2013) 209
6. T. S. Santra, T. K. Bhattacharyya, P. Mishra, F. G. Tseng, T. K. Barik, *Sci. Adv. Mater*. 4 (1) (2012) 110
7. Y. J. Xue, D. Zhu, F. Zhao, *J. Mater. Sci*. 39 (2004) 4063
8. E. Aghaie, A. Najafi, H. Maleki-Ghaleh, H. Mohebi, *Surf. Eng*. 29 (3) (2013) 177
9. T. Borkar, S.P. Harimkar, *Surf. Coat. Technol*. 205 (17-18) (2011) 4124
10. H. Ogihara, M. Safuan, T. Saji, *Sur f. Coat. Technol*. 212 (2012) 180
11. I. Zamblau, S. Varvara, L. M. Muresan, *J. Mater. Sci.* 46 (20) (2011) 6484
12. T. Borkar, S. Harimkar, *Surf. Eng*. 27 (7) (2011) 524
13. K. A. Kumar, P. Mohan, G. P. Kalaignan, V. S. Muralidharan, *J. Nanosci. Nanotechnol*. 12 (11) (2012) 8364
14. S.Y. Hung, *J. Micrmech. Microeng*. 19(1)(2009) 015009
15. S. Meenu, V. K. W. Grips, K. S. Rajam, *Appl. Surf. Sci*. 253(8)(2007)3814
16. P. Suphantharida, K. Osseo-Asare, *J. Electrochem. Soc*. 151(10)(2004)G658.
17. R. Schmechel, H. Winkler, X. M. Li, M. Kennedy, M. Kolbe, A. Benker, *Scripta. Mater*. 44(8–9) (2001) 1213
18. C. L. Campos, C. L. Laboy, M. Aponte, *Abstr. Pap. Am. Chem*. S. 225(2003) U643
19. G. Carac, L. Benea, C. Iticescu, T. Lampke, S. Steinhauser, B. Wielage. *Surf. Eng*. 20(5)(2004) 353
20. O. Mitoseriu, C. Iticescu, G. Carac, *Rev. Chim*. 55 (7)(2004) 525
21. S. Balathandan, S. K. Seshadri, *Met. Finish.* (1994),49-53
22. X. H. Yu, H.Y. Wang, Z.R. Yang, P. Yin, X.Q. Xin, *Appl. Surf. Sci*. 158 (3-4) (2000) 335
23. S. Meenu, V. K. W. Grips, K. S. Rajam, *Appl. Surf. Sci.* 257 (2010) 717
24. S. T. Aruna, C. N. Bindu, V. E. Selvi, V. K. W. Grips, K. S. Rajam, *Surf. Coat. Technol*.200 (2006) 6871
25. Y. J. Xue, H. B. Liu, M. M. Lan, J. S. Li, H. Li, *Surf. Coat. Technol*.204(21-22) (2010) 3539
26. Q. Y. Feng, T. J. Li, H. Y. Yue, K. Qi, F. D. Bai, J. Z. Jin, *Appl. Surf. Sci*. 254 (2008) 2262
27. S. Mohajeri, A. Dolati, S. Rezagholibeiki, *Mater. Chem. Phys*. 129 (2011) 746
28. S. M. LariBaghal, A. Amadeh, M. HeydarzadehSohi, S.M.M. Hadavi, *Mater. Sci. Eng*. A 559 (2013) 583
29. B. Bakhit, A. Akbari, *J. Alloy Compd*. 560 (2013) 92–104
30. Q. Y. Feng, T. J. Li, H. Y. Yue, K. Qi, F. D. Bai, J. Z. Jin, *Surf. Coat. Technol*. 202 (2008) 4137
31. L. Shi, C. F. Sun, P. G. F. Zhou, W. Liu, *Appl. Surf. Sci*.252 (2006) 3591
32. N. Guglielmi, *J. Electrochem. Soc*. 119 (1972) 1009
33. N. S. Qu, D. Zhu, K. C. Chan, *Scripta. Mater*. 54 (2006) 1421
34. K. C. Chan, N.S. Qu, D. Zhu, *Surf. Coat. Technol*. 99(1-2) (1998) 69
35. J. P. Bonino, S. Loubiere, A. Rousset, *J. Appl. Electrochem*. 28(11) (1998) 1227
36. C. F. Malfatti, H. M. Veit, T. L. Menezes, J. Z. Ferreira, J. S. Rodriguês,J. P. Bonino, *Surf. Coat. Technol.* 201(14) (2007) 6318
37. Y. J. Xue, X. Z. Jia, Y. W. Zhou, W. M. Ma, J. S. Li, *Surf. Coat. Technol*. 200 (2006) 5677